Analytical Biochemistry 534 (2017) 99–107

Contents lists available at ScienceDirect

Analytical Biochemistry

journal homepage: www.elsevier.com/locate/yabio

Development of carbon–graphene-based aptamer biosensor for EN2 protein detection

Kalpana Settu [a], Jen-Tsai Liu [b], Ching-Jung Chen [c], Jang-Zern Tsai [d, *]

[a] Department of Electrical Engineering, National Taipei University, Sanxia, Taiwan
[b] College of Materials Sciences and Opto-electronics, University of Chinese Academy of Sciences, Beijing, China
[c] School of Electronic and Communication Engineering, University of Chinese Academy of Sciences, Beijing, China
[d] Department of Electrical Engineering, National Central University, Jhongli, Taiwan

ARTICLE INFO

Article history:
Received 1 March 2017
Received in revised form
1 July 2017
Accepted 10 July 2017
Available online 11 July 2017

Keywords:
Electrochemical
Biosensor
Graphene
Aptamer
EN2 protein
Screen-printing

ABSTRACT

In this study, we developed a screen-printed carbon–graphene-based electrochemical biosensor for EN2 protein detection. The engrailed-2 (EN2) protein, a biomarker for prostate cancer, is known to be a strong binder to a specific DNA sequence (5′-TAATTA-3′) to regulate transcription. To take advantage of this intrinsic property, aptamer probes with TAATTA sequence was immobilized onto the screen-printed carbon–graphene electrode surface via EDC–NHS coupling approach. Cyclic voltammetry (CV) of the electrochemical measurement technique was employed for the quantitative detection of EN2 protein. The hindrance to the redox reaction of potassium ferricyanide on the biosensor surface due to the binding of the immobilized aptamer with its target EN2 protein quantified the protein concentration. Under optimum conditions, the aptamer biosensor can detect EN2 protein over a linear range from 35 to 185 nM with a detection limit of 38.5 nM.

Introduction

Prostate cancer is one of the most common malignancy among men in many countries and is a leading cause of death [1]. There are several methods for early screening and diagnosis of prostate cancer, including prostate imaging, biopsy, and prostate-specific antigen (PSA) screening [2,3]. The combination of serum PSA measurements and digital rectal examination (DRE) has usually been utilized for early screening of prostate cancer [4]. However, PSA is a prostate-specific marker but not a prostate cancer-specific marker and is frequently raised in noncancerous conditions, such as benign prostatic hyperplasia (BPH) and prostatitis [5–7]. This implies that the PSA screening lacks both sensitivity and specificity to accurately detect the presence of prostate cancer. Therefore, the development of a diagnostic method based on a biomarker more powerful than PSA has been strongly demanded.

A number of genes are involved in early embryonic development and are subsequently re-expressed in cancer. For example, the HOX genes are a family of homeodomain-containing transcription factors that determine the early identity of cells and tissues [7–10]. Engrailed-2 (EN2), a transcriptional repressor and a member of the HOX group, shows a very high degree of functional conservation during embryonic development and hence is a potential biomarker for several cancers, including breast cancer, ovarian cancer, bladder cancer, and prostate cancer [11–14]. Morgan et al. (2011) reported that full-length Engrailed-2 (EN2) protein can be released from prostatic cancer acini and ducts and be detected in the urine. Their cohort study resulted in a sensitivity of 66% and a specificity of 88.2% on the basis of EN2 detection with a threshold level of 42.5 μg/L [13,14]. Therefore, the presence of EN2 in urine is highly predictive of prostate cancer, indicating that EN2 is a potential diagnostic biomarker.

Enzyme-linked immunosorbent assay (ELISA) is a widely used technique for protein detection [13]. However, ELISAs have a number of disadvantages, such as requirements for relatively expensive test kits, bulky plate readers, and lengthy procedures [15]. Biosensor technologies have been used as potential alternatives to circumvent the bottlenecks of traditional methods because

* Corresponding author. Department of Electrical Engineering, National Central University, Jhongli, 32001, Taiwan.
E-mail address: jztsai@ee.ncu.edu.tw (J.-Z. Tsai).

http://dx.doi.org/10.1016/j.ab.2017.07.012
0003-2697/

of their rapid response time, sensitivity, portability, and ease of use. Biosensors that use an aptamer as a specific recognition part have become an area of research interest. Aptamers are single-stranded DNA (ssDNA) or RNA oligonucleotides that form sequence-defined unique structures with binding affinities for specific targets [16,17]. Several characteristics of aptamers make them attractive recognition receptors for bio-sensing assay development, such as stability, ease of synthesis and labeling, low production cost, and high target binding affinity and specificity [18–21]. The target molecules of an aptamer can be proteins, small organic molecules, metal ions, or even whole cells or microorganisms [19,22–25]. Aptamer biosensors provide a quick, cost-effective and sensitive platform for screening methods with minimal sample preparation [26,27].

Eelectrochemical aptamer sensors have attracted interests, due to their combined advantages of sensitivity, miniaturization capability, and low cost, as well as high stability [28–30]. An ideal biosensor should have a high signal/noise (S/N) ratio, a low detection limit and a broad linear detection range of the analyte concentration [31]. Graphene has received special attention in the development of advanced biosensing systems. Recently, a new, low-cost and efficient screen-printed carbon–graphene paste electrode (SPCGE) has been developed for the electrochemical detection of H_2O_2, NAD^+/NADH and $(Fe(CN)_6^{3-/4-})$ redox couples [32]. The direct incorporation of graphene into the carbon paste for electrode fabrication resulted in enhanced electrochemical response attributed to the increased reactive surface area, electronic mobility and electron transfer rate. As a result, relatively wide dynamic ranges, high sensitivities, low detection limits and high reproducibility could be achieved.

In this study, an electrochemical aptamer biosensor based on screen-printed electrodes of carbon–graphene paste was developed for the detection of EN2 protein. The electrodes of the biosensor were formed by screen-printing a mixture of graphene and carbon paste on a polycarbonate substrate. EN2 protein-specific aptamer sequence [33] with amine linker was immobilized on the screen-printed electrode surface. Finally, cyclic voltammetry (CV) was used to quantify the EN2 protein concentration with the developed aptamer biosensor.

Materials and methods

Reagents

N-hydroxysulfosuccinimide (sulfo-NHS or simply NHS), 1-ethyl-3-(3-dimethylamino-propyl) carbodiimide hydrochloride (EDC), and stearic acid were purchased from Sigma-Aldrich Corp. (St. Louis, MO, USA). The analytical grade hydrochloric acid (HCl) was obtained from Avantor Performance Materials (Center Valley, PA, USA). Calcium carbonate ($CaCO_3$) was supplied by Formosa Plastics Corporation (Taipei, Taiwan). Polyvinyl chloride (PVC) substrate was obtained from Jan Yan Print Int'l Corporation (Taoyuan, Taiwan). Carbon paste was purchased from Gwent Electronic Materials Ltd. (Pontypool, UK). Graphene powder was obtained from Enerage Inc. (Taipei, Taiwan). Deionized water (18.2 MΩ/cm) obtained from a Lotun ultrapure water purification system (Lotun Technic Co., Ltd., Taipei, Taiwan) and filtered through a 0.22-μm Millipak 40 Membrane (Millipore Corp., Bedford, MA, USA) was used in all the experiments. DNA aptamer probe used in this study was obtained from MD-Bio Inc. (Taipei, Taiwan); it was a 46-mer base sequence of 5′-NH_2-AAA AAA AAA ACG TGT AAT TAC CTC CAG AAG GAG AGG TAA TTA CACG-3′. The estimated dissociation constant of the aptamer was 66 nM [33].

Fabrication of carboxyl-enriched screen-printed carbon–graphene electrodes (COOH-SPCGE)

Firstly, 0.135 g graphene powder, 0.3 g $CaCO_3$ powder and 0.43 g stearic acid were well mixed with 9 g of carbon paste by using an IKA RW 20 digital stirrer (IKA Works Inc., NC, USA). Then, this carbon–graphene paste containing $CaCO_3$ and stearic acid was used to print electrodes on a PVC substrate by utilizing a TY-300 FAT screen-printing machine (ATMA CHAMP Ent. Corp., Taipei, Taiwan). After being dried by an oven at 60 °C for 30 min, the electrodes were immersed in 1-M HCl for 1 h for the $CaCO_3$ to dissolve. Finally, the electrodes were rinsed with deionized water and dried in air for further use. An electrode thus formed was called a carboxyl-enriched porous screen-printed carbon–graphene electrode (COOH-SPCGE).

Immobilization of aptamer on COOH-SPCGE surface

DNA probe was covalently attached to the carboxyl outer layer of the electrode surface through EDC–NHS chemistry. Firstly, the electrode was immersed for 15 min in a 10-mM phosphate buffer solution (PBS) of pH 6.0 containing 2-mM EDC and 5-mM sulfo-NHS. Secondly, a 10-mM PBS of pH 7.4 containing aptamer probe of a 1-μM concentration was dropped onto the electrode surface, which was then left at room temperature for an optimum length of time (namely 3 h, described in 3.2.1). Then the electrode was washed with DI water to remove unbound aptamer probes. The preparation process of the aptamer biosensor is schematically shown in Fig. 1.

Surface morphology and composition analysis

To verify the aptamer immobilization result, the composition of the electrode surface after aptamer immobilization was observed with a scanning electron microscope (SEM, Model S-3500N, Hitachi Ltd., Tokyo, Japan) coupled with an energy dispersive X-ray spectroscope (EDS, Model EX-200, HORIBA Ltd., Kyoto, Japan).

Performance evaluation of the biosensor in EN2 concentration measurement

The performance of the proposed biosensor was evaluated with standard EN2 protein solutions of different concentrations

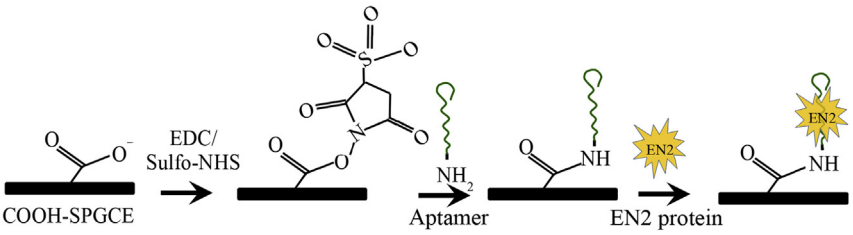

Fig. 1. Schematic representation of the aptamer biosensor preparation.

prepared in 10-mM PBSs of an optimum pH level (namely pH 7.5, described in 3.2.2) containing NaCl of an optimum concentration (namely 0.2 M, described in 3.2.3). The measurement of EN2 concentration comprises a first step of EN2 binding and a second step of CV scan. In Step 1, each of the prepared EN2 protein solutions was dropped on an aptamer-immobilized biosensor followed by an optimum binding time (namely 30-min, described in 3.2.4) at an optimum temperature (namely 25 °C, described in 3.2.5) for the EN2 protein to bind to the aptamer. Afterward, the biosensors were washed with a pH-7.5 PBS to remove unbound protein. In Step 2, cyclic voltammetry was carried out with each biosensor in a 10-mM PBS of an optimum pH level (namely pH 7.5, described in 3.2.6) with 0.1-M potassium ferricyanide ($K_3Fe(CN)_6$) as the redox probe. The CV scanning was conducted over a potential range from −0.9 to +0.9 V at a scan rate of 50 mV/s. Finally, the calibration curve of CV response current vs. EN2 concentration was obtained and the detection range and the limit of detection were determined.

The CV measurement was carried out using an IM6-eX electrochemical workstation (ZAHNER-Elektrik GmbH & Co. KG, Germany). One of the two contact pads of the biosensor was connected to the test and sense probes and the other was connected to the reference and counter probes on the IM6-eX electrochemical workstation.

Results and discussion

Characterization of DNA immobilization

The covalent immobilization of aptamer probe onto the electrode surface was obtained via 1-ethyl-3-(3-dimethylaminopropyl) carbodiimide (EDC) and N-hydrosulfosuccinimide (NHS) cross-linking reaction. Although physical adsorption is a simpler way to attach DNA onto a solid surface, the attached DNA on the solid surface is not well ordered or tightly bound. By contrast, the EDC–NHS covalent bonding approach produces a more ordered DNA immobilization with a higher DNA surface density on the electrode surface [34,35]. Amine-modified DNA aptamer was used in this work to anchor amine groups from the 5′ terminal to carboxylate groups of stearic acid to get a more orderly aptamer on the electrode surface. In the presence of EDC and NHS, the aptamer modified with amine linker at 5′ terminal forms a peptide bond with the COO− groups from stearic acid on the electrode surface. The surface modification was characterized by SEM/EDS and cyclic voltammetric measurements described below.

SEM/EDS

The result of the electrode surface modification with EDC–NHS and aptamer was analyzed with scanning electron microscopy/

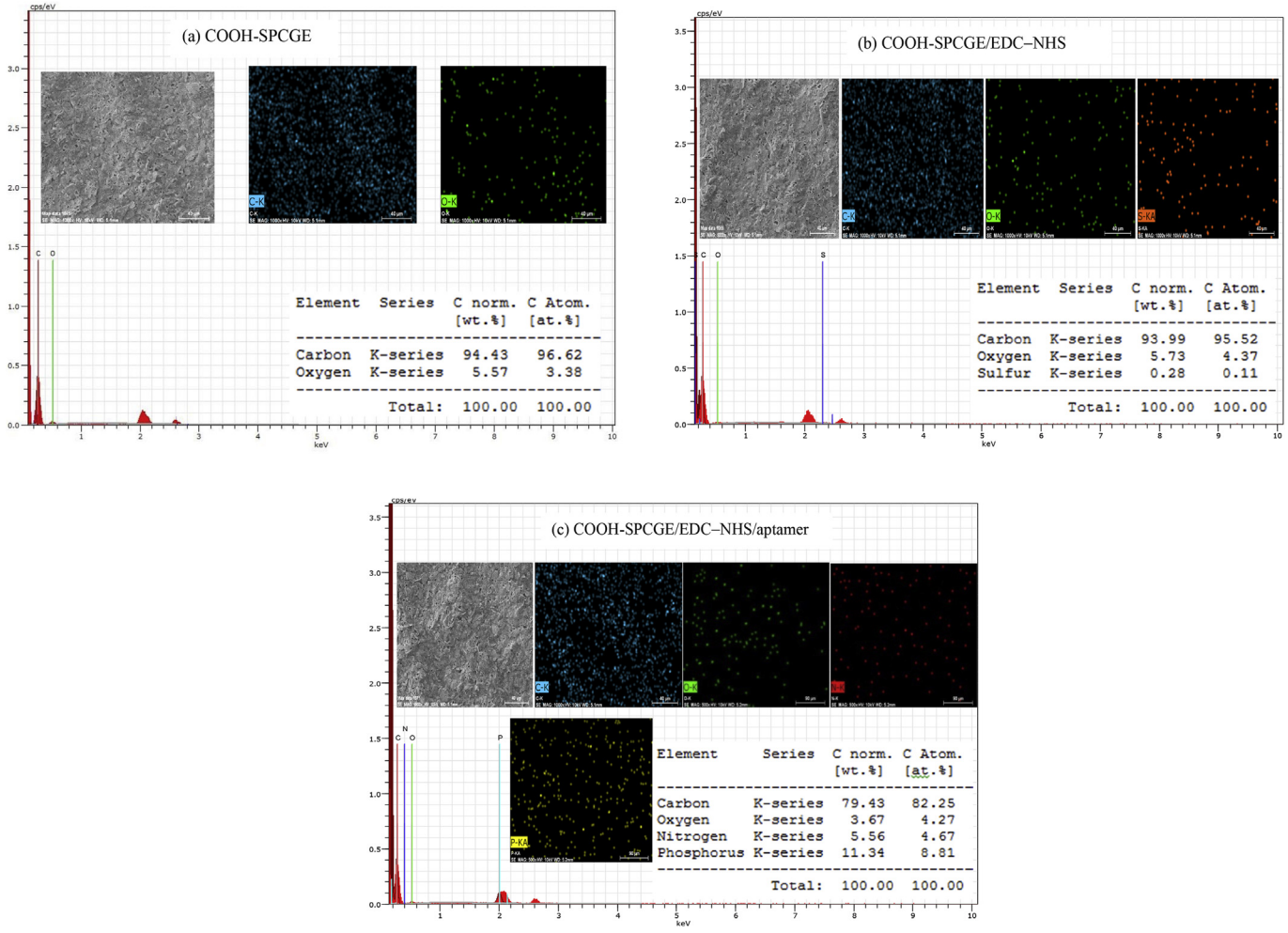

Fig. 2. SEM/EDS mapping analysis on (a) COOH-SPCGE, (b) COOH-SPCGE/EDC–NHS, (c) COOH-SPCGE/EDC–NHS/aptamer.

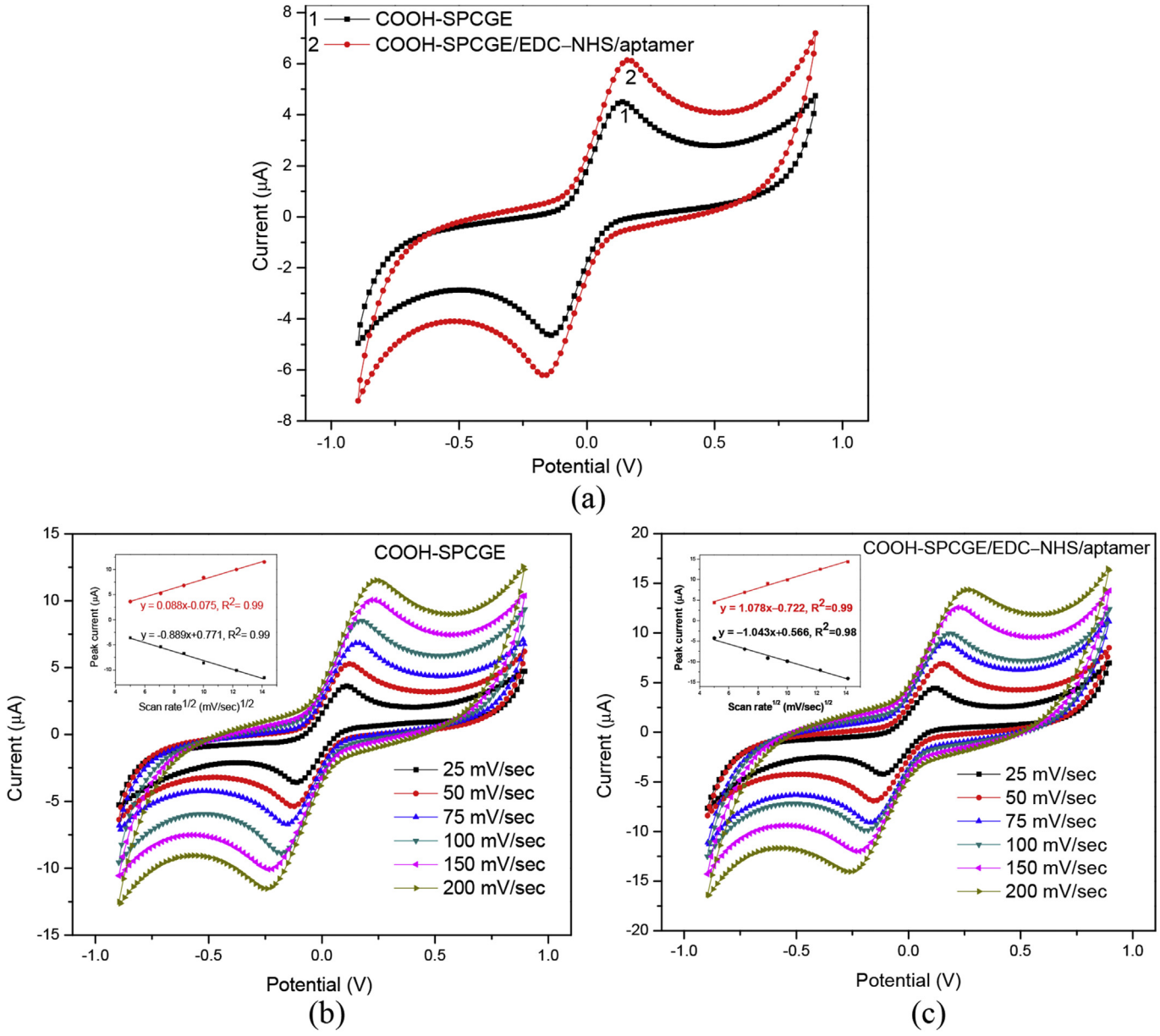

Fig. 3. The results of CV characterization. (a) On bare COOH-SPCGE and aptamer-immobilized COOH-SPCGE; (b) on bare COOH-SPCGE, various scan rates; (c) on aptamer-immobilized COOH-SPCGE, various scan rates.

energy dispersive X-ray spectroscopy (SEM/EDS) for confirming the presence of DNA. Fig. 2(a) indicates that the COOH-SPCGE surface was composed of 94.43 wt% of carbon and 5.57 wt% of oxygen. The presence of oxygen element reflected the addition of stearic acid powder in the carbon–graphene paste for creating the carboxyl groups on electrode surface. Fig. 2(b) indicates that, after being dropped with EDC and sulfo-NHS, the electrode surface contained sulfur along with carbon and oxygen elements (93.99 wt% of C, 5.73 wt% of O, and 0.28 wt% of S). The presence of sulfur (from sulfo-NHS) on the electrode surface proved that the carboxyl groups on the electrode surface were successfully activated by EDC–sulfo-NHS. Fig. 2(c) shows that, after being modified with aptamer, the electrode surface consisted of 79.43 wt% of carbon, 3.67 wt% of oxygen, 5.56 wt% of nitrogen and 11.34 wt% of phosphorous. The presence of nitrogen and phosphorus, from the amine linker and the sugar-phosphate backbone of the DNA, respectively, reflected a successful immobilization of the aptamer on the electrode surface. In all these cases, the SEM pictures and EDS mapping analyses showed a homogeneous distribution of elements over the sample surface, demonstrating a successful modification of the electrode surface.

Cyclic voltammetric characterization

The electron transfer property of the electrode after aptamer immobilization was confirmed using cyclic voltammetry with a 10-mM PBS solution containing 0.1-M $K_3Fe(CN)_6$ at a scan rate of 50 mV/s.

The electrode reaction mechanisms of the electroactive species at the electrode surface can be verified by the CV measurement. Fig. 3(a) illustrates cyclic voltammograms of the bare COOH-SPCGE and aptamer modified COOH-SPCGE. The electrochemical behaviors of the electroactive $Fe(CN)_6^{3-/4-}$ redox couple was used to

reflect the electron transfer characteristic of the modified electrode surface. As for the bare COOH-SPCGE (Curve 1, Fig. 3(a)), a pair of redox peaks for $Fe(CN)_6^{3-/4-}$ appeared at −0.121 V and +0.121 V at a scan rate (ν) of 50 mV/s to give a peak potential difference ΔE_p of 0.242 V. As shown in Fig. 3(a) (curve 2), the redox peak current of the aptamer-immobilized COOH-SPCGE increased remarkably. Our experiment result is consistent with the literature [36,37]. According to these reports, the increase in peak current after aptamer immobilization could be attributed to the increase of electron transfer through the DNA chain [37], whose negatively charged phosphate backbone [38] could adsorb K^+ to its surface. With a stronger affinity to the adsorbed K^+ ions, more $Fe(CN)_6^{4-}$ anions than other anions were attracted towards the electrode surface thereby causing an increase in the peak current of $Fe(CN)_6^{3-/4-}$ [36]. The increased current response due to aptamer immobilization implied that the aptamer had been immobilized successfully on the electrode surface.

Fig. 3b and c shows the cyclic voltammetric behavior of the bare COOH-SPCGE and aptamer-modified COOH-SPCGE, respectively, at various scan rates. In both cases, the ΔE_p increased with the increased scan rate and the peak current was directly proportional to the square root of the scan rate (shown in the insets of Fig. 3b and c), which indicates a diffusional process at the electrode surface [39]. The diffusion coefficient D_0 was calculated from the linear relationship between the peak current i_p and the square root of the scan rate v according to the Randles–Sevcik equation:

$$i_p = \left(2.69 \times 10^5\right) n^{3/2} A D_0^{1/2} C v^{1/2} \quad (1)$$

where n is the number of electrons transferred, A the area of the working electrode, and C the concentration of the redox species in the solution. The diffusion coefficient of the electroactive species to or from the electrode surface was calculated from Eqn (1) by using cathodic peak currents. The calculated diffusion coefficients for the bare COOH-SPCGE and aptamer-immobilized COOH-SPCGE were 5.62×10^{-11} and 8.84×10^{-11} cm^2/s, respectively. Diffusion coefficient for the modified aptamer-immobilized COOH-SPCGE was significantly greater than the bare COOH-SPCGE ($P < 0.01$).

Optimizations for electrochemical measurement

Optimization of aptamer immobilization time

As stated in 2.3, an optimum length of time was desired for immobilizing aptamer on the COOH-SPCGE/EDC–NHS surface. To this end, a preliminary CV experiment was conducted by characterizing aptamer-immobilized electrodes, i.e., COOH-SPCGE/EDC–NHS/aptamer, that had been made with different lengths of aptamer immobilization time. The resultant CV peak currents are shown in Fig. 4. The CV peak current increased with increased length of immobilization time. That means a longer immobilization time resulted in a larger amount of aptamer probes immobilized onto the electrode surface. After 3 h of exposure to the aptamer probes, the active sites of electrode surface were presumably fully attached with aptamer probes. So the CV peak current only had insubstantial change ($p > 0.05$, one-way ANOVA) beyond 3 h of immobilization time. Therefore 3 h was chosen as the optimum aptamer immobilization time, that is, the length of time from dropping aptamer-containing PBS on the COOH-SPCGE/EDC–NHS to washing it with DI water.

Optimization of pH of the PBS for protein–aptamer binding

The pH of the PBS for preparing a standard EN2 protein solution, mentioned in 2.5, might have an effect on the binding efficiency of the EN2 protein to the aptamer on the electrode surface, which affected the sensitivity of the biosensor. To determine the optimum pH of the PBS, a preliminary experiment was conducted by using PBSs of different pH levels to prepare EN2 protein solutions and then performing CV assay of these solutions with the biosensors. These EN2 protein solutions were all 185 nM in concentration and were prepared at room temperature. Fig. 5 shows the resultant CV peak current with respect to the pH level of the PBS. The CV peak current was the lowest for the EN2 protein solution with pH-7.5 PBS and it is significantly different ($p < 0.05$, t-test) from that with pH-7 PBS. This indicates that EN2 protein binds to aptamer more easily at pH 7.5. Previous studies [40] have reported that in a more acidic environment, the protonation reaction of the phosphodiester of the DNA can reduce the solubility of the DNA molecule, which eventually decreases the DNA hybridization. In a more basic medium, DNA hybridization also decreased and hence the response of DNA biosensor was also weakened [41]. Therefore, 7.5 was selected as the optimum pH of the PBS for EN2 protein–aptamer binding.

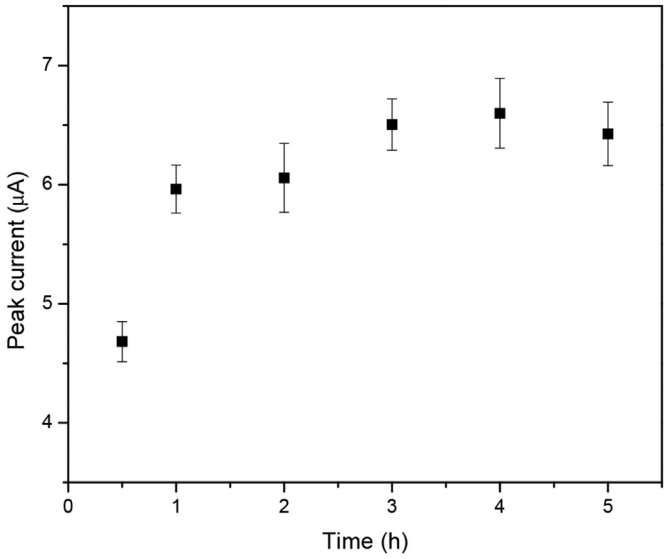

Fig. 4. Experimental result showing the effect of aptamer probe immobilization time on CV peak current. Each of the error bars denotes the standard deviation of 4 measurements.

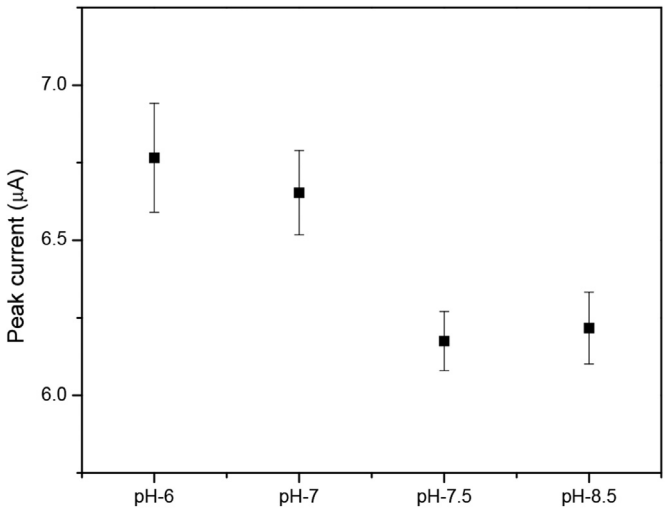

Fig. 5. Experimental result showing the effect of the pH of PBS on EN2 protein–aptamer binding. Each of the error bars denotes the standard deviation of 4 measurements.

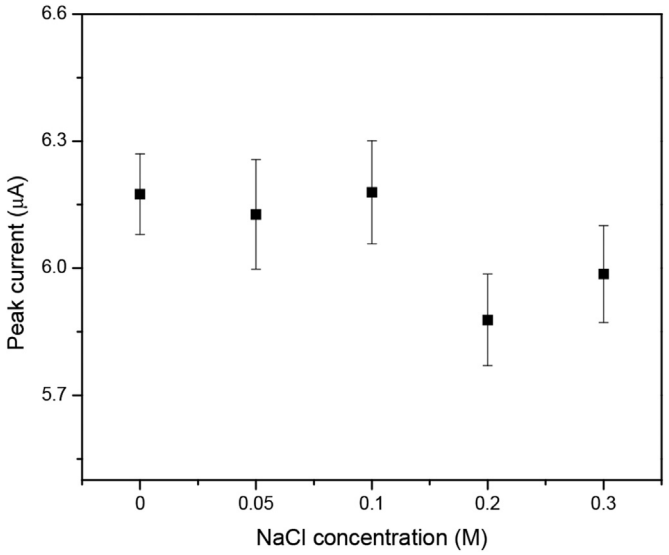

Fig. 6. Experimental result showing the effect of sodium ion concentration on EN2 protein–aptamer binding. Each of the error bars denotes the standard deviation of 4 measurements.

Optimization of the sodium ion concentration

It has been known that a higher DNA hybridization rate can be achieved in the presence of Na^+ ion due to its small size and high affinity to DNA phosphodiester chain to reduce the electrostatic repulsion between DNA molecules [40]. Fig. 6 shows the results of CV when different NaCl concentrations were used for preparing the standard EN2 protein solutions (mentioned in 2.5) in a preliminary experiment to determine the optimum NACl concentration. It evidences that sodium ion concentration has an effect on the biosensor response. A possible explanation for this is that with a certain amount of sodium ions in the solution, the electrostatic repulsion between aptamer molecules decreased and thus the protein–aptamer binding reaction was enhanced. As shown in Fig. 6, when the NaCl concentration was increased to 0.2 M, the peak current became significantly lower ($p < 0.05$, t-test). Hence, the optimum NaCl concentration was determined to be 0.2 M, at which the biosensor gave the highest degree of protein–aptamer binding.

Optimization of the time for protein–aptamer binding

As stated in 2.5, in Step 1 of EN2 concentration measurement, the EN2 protein and the aptamer needed a length of time to bind to each other after the EN2 protein solution was dropped on the aptamer-modified surface of the biosensor. On the other hand, too long a binding time is meaningless. Hence, the optimum binding time is the shortest length of time within which the binding of protein and aptamer can reach a saturated level. Fig. 7 shows the CV peak current of a preliminary experiment for finding the optimum binding time. It illustrates that the CV peak currents tended to level off with a binding time longer than 30 min. The t-test shows there was no significant change in peak current with a binding time longer than 30 min. Thus, 30 min was chosen as the optimum binding time.

Optimization of the temperature for protein–aptamer binding

Temperature might be a factor on protein–aptamer binding. Fig. 8 shows the result of a preliminary experiment for finding the optimum temperature for the binding time in Step 1 of EN2 concentration measurement mentioned in 2.5. As can be seen in this figure, the CV peak current with EN2 (when the temperature was 4, 25, or 37 °C) was significantly lower ($p < 0.05$, t-test) from the one without EN2. On the other hand, one-way ANOVA shows that the peak currents at different temperatures (4, 25, 37 °C) were not significantly different. For the sake of convenience, 25 °C, i.e., the room temperature, was chosen as the optimum temperature.

Optimization of the pH for cyclic voltammetry

Fig. 9 illustrates the CV response of the biosensor as a function of the pH of PBS. The highest CV peak current was attained at pH 7.5. Therefore, the optimum pH of the PBS for cyclic voltammetry was determined to be 7.5. Indeed, all the preliminary experiments mentioned in 3.2.2–3.2.5 all used this pH for the PBSs.

EN2 protein detection

Direct assay

The optimized aptamer biosensor was used to detect various

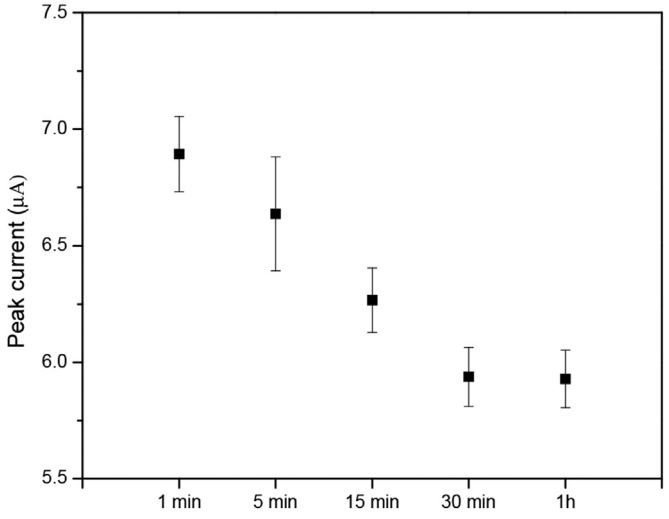

Fig. 7. Experimental result showing the effect of binding time on EN2 protein–aptamer binding. Each of the error bars denotes the standard deviation of 4 measurements.

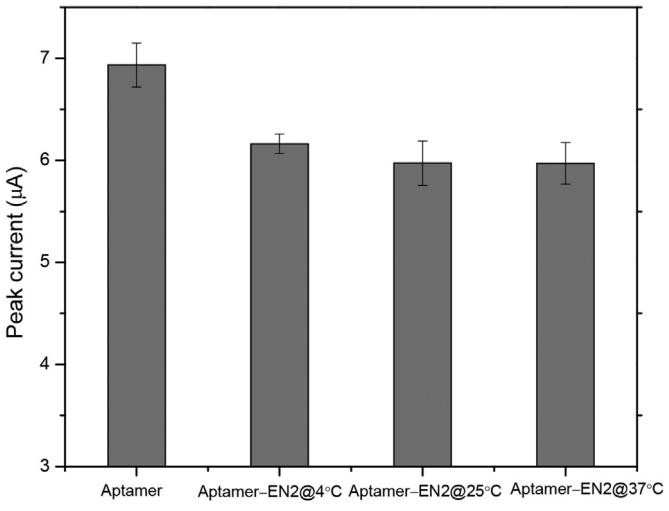

Fig. 8. Experimental result showing the effect of temperature on EN2 protein–aptamer binding. Each of the error bars denotes the standard deviation of 4 measurements.

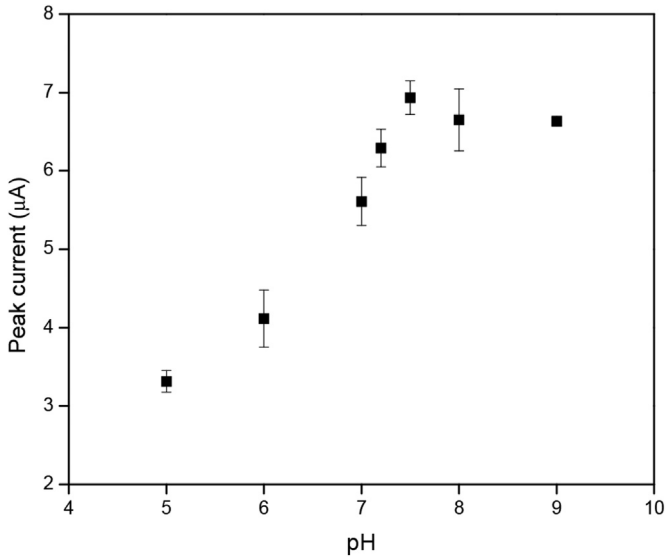

Fig. 9. Experimental result showing the effect of the pH of PBS on the response of the aptamer-immobilized biosensor. Each of the error bars denotes the standard deviation of 4 measurements. The peak currents with different pH values were compared with *t*-test. The peak current with pH 7.5 was significantly higher ($p < 0.05$) than those with lower pH values. Its mean was higher than those with higher pH values.

concentrations of EN2 protein (35 nM–350 nM) by measuring CV peak current. The hindrance of the redox reaction of $K_3Fe(CN)_6$ on the electrode surface due to the target EN2 protein bound to the immobilized aptamer probe caused the current response to decrease with increased EN2 protein concentrations, as can be seen from Fig. 10. The CV peak current response of the aptamer biosensor exhibited a linear range from 35 nM to 185 nM, and the linear equation was I(μA) = 6.648 − 0.00383 [EN2 protein](nM) with a coefficient of determination R^2 = 0.94. The calculated limit of detection (LOD) was 38.5 nM. The LOD is not yet sufficient for clinical diagnostics and hence further investigation on signal enhancement is required in order to improve the LOD.

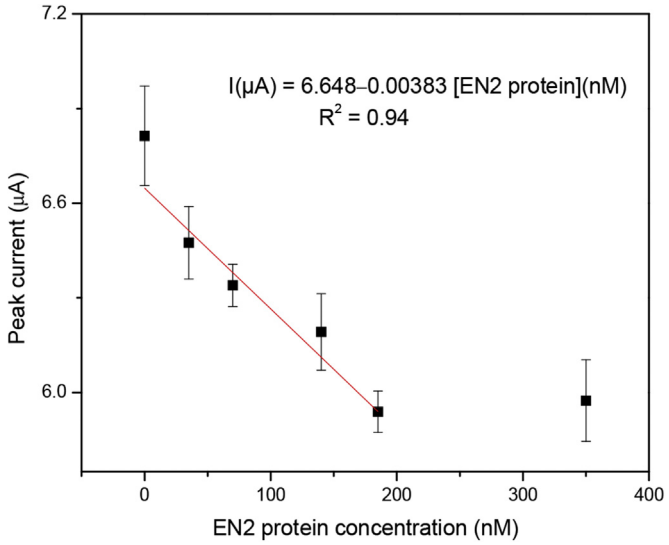

Fig. 10. Cyclic voltammetry peak current vs. EN2 protein concentration in PBS. The red straight line represents the linear regression line. Each of the error bars denotes the standard deviation of 4 measurements. (For interpretation of the references to colour in this figure legend, the reader is referred to the web version of this article.)

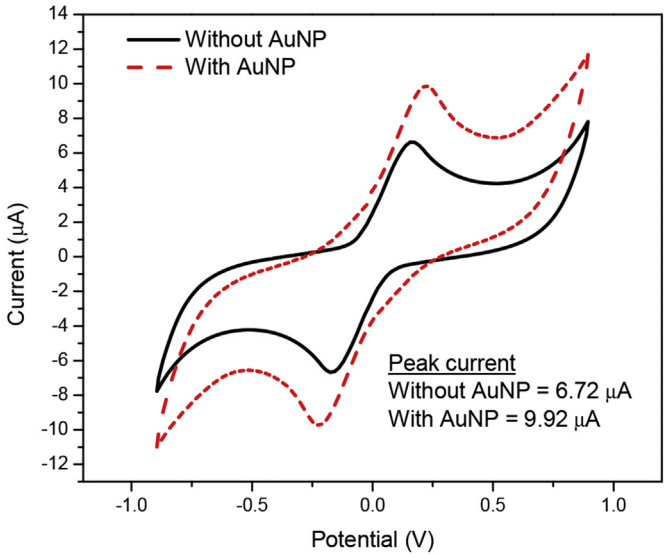

Fig. 11. Cyclic voltammogram of aptamer-immobilized sensor with and without AuNP coating.

AuNP-enhanced assay

In order to improve the sensitivity and detection limit, signal enhancement by gold nanoparticles of 5-nm diameter was performed. Different-sized AuNPs could produce different levels of signal enhancement [42]. While the aptamer recognition layer was formed on the electrode surface and small-sized AuNPs could possess the advantage of better diffusion to the surface. In this study, we chose 5-nm AuNPs. A 20 μl of gold colloid was dropped onto the aptamer-immobilized electrode surface and dried in air. As shown in Fig. 11, the CV current response enhanced significantly after AuNPs coating. The CV peak current value with and without AuNPs coating was 9.92 and 7.72 μA, respectively. This shows that the electrochemical signal was enhanced by about 1.5 times after AuNP assay. Hence, AuNPs-coated sensor was employed to detect EN2 protein.

Fig. 12 shows the CV peak current change (ΔI) vs EN2 concentration in direct assay (a) and AuNP-enhanced assay (b). Peak current change, $\Delta I = I - I_0$, where I_0 and I are the peak currents obtained from PBS without and with EN2 protein, respectively. The signal enhancement by AuNP improved the detection range from 35–185 nM to 20–350 nM and the LOD from 38.5 nM to 19.4 nM.

Recently, Lee et al. (2015) developed a gold nanoparticles-based electrochemical biosensor with gold electrodes for the detection of EN2 protein [33]. The detection range of their sensor is 10 fM to 1 nM with an LOD of 5.62 fM. However, it involves a high cost for sensor material (gold). In contrary, the method proposed in our study demonstrates the possibility of detecting EN2 protein at a low cost. To the best of our knowledge, no other study for the detection of EN2 protein has been reported.

Conclusion

We have demonstrated the construction of a screen-printed carbon–graphene-based electrochemical aptamer biosensor for detecting EN2 protein at a nanomolar level, using a specific DNA aptamer probe immobilized on the electrode surface. The electrochemical measurements successfully detected the EN2 protein over a linear range from 35 to 185 nM with a detection limit of 33.8 nM. The proposed carbon–graphene-based electrochemical biosensor holds great promise in clinical diagnosis. Our future study aims to

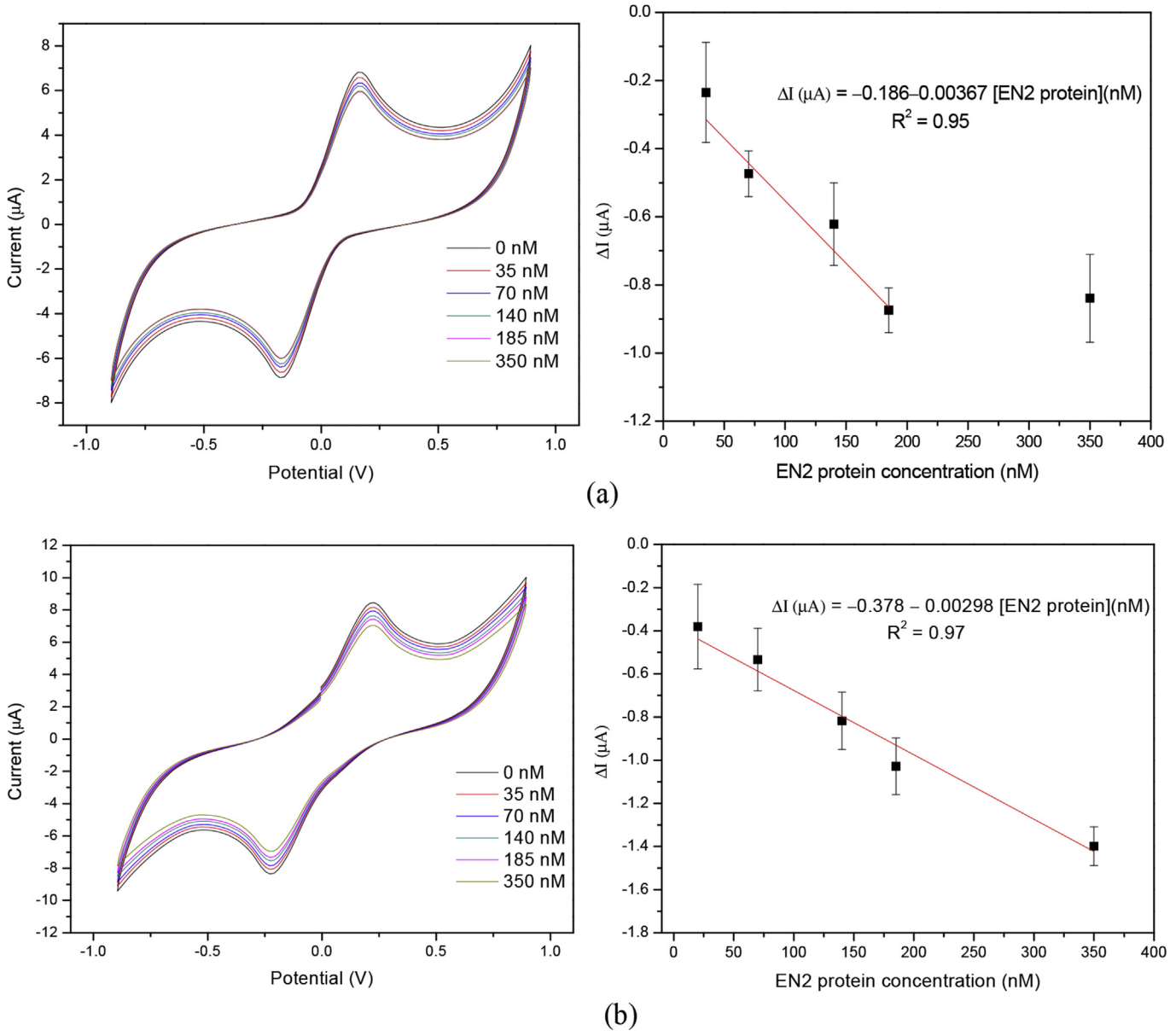

Fig. 12. Cyclic voltammograms of EN2 protein detection and the corresponding change of the peak current vs. EN2 protein concentration in PBSs with (a) direct assay and (b) AuNP-enhanced assay. The red straight lines represent the linear regression lines. Each of the error bars denotes the standard deviation of 4 measurements.

improve the detection limit to the sub-nanomolar level through investigation and improvement with different electrode materials or electrode configurations or employing different electrochemical detection techniques. Considering possible interferences from other electroactive substances or proteins in the urine, we will also conduct an interference study to confirm the developed biosensor's selectivity to EN2 protein.

Acknowledgments

This research was supported under grants MOST 105-2221-E-008-089 and MOST 104-2221-E-008-073 by the Ministry of Science and Technology, Taiwan.

References

[1] R. Siegel, E. Ward, O. Brawley, A. Jemal, The impact of eliminating socioeconomic and racial disparities on premature cancer deaths, CA Cancer J. Clin. 61 (2011) 212–236.
[2] R. Bryant, T. Pawlowski, J. Catto, G. Marsden, R. Vessella, B. Rhees, C. Kuslich, T. Visakorpi, F.C. Hamdy, Changes in circulating microRNA levels associated with prostate cancer, Br. J. Cancer 106 (2012) 768–774.
[3] J.R. Prensner, M.A. Rubin, J.T. Wei, A.M. Chinnaiyan, Beyond PSA: the next generation of prostate cancer biomarkers, Sci. Transl. Med. 4 (2012), 127rv3.
[4] A. Wolf, R.C. Wender, R.B. Etzioni, I.M. Thompson, A.V. D'Amico, R.J. Volk, et al., American Cancer Society guideline for the early detection of prostate cancer: update 2010, CA Cancer J. Clin. 60 (2010) 70–98.
[5] H. Lilja, D. Ulmert, A.J. Vickers, Prostate-specific antigen and prostate cancer: prediction, detection and monitoring, Nat. Rev. Cancer 8 (2008) 268–278.
[6] G.L. Andriole, E.D. Crawford, R.L. Grubb, S.S. Buys, D. Chia, T.R. Church, et al., Mortality results from a randomized prostate-cancer screening trial, N. Engl. J. Med. 360 (2009) 1310–1319.
[7] J. Hugosson, S. Carlsson, G. Aus, S. Bergdahl, A. Khatami, P. Lodding, et al., Mortality results from the Göteborg randomised population-based prostate-cancer screening trial, Lancet Oncol. 11 (2010) 725–732.
[8] T.R. Daniels, Neacato, II, J.A. Rodriguez, H.S. Pandha, R. Morgan, M.L. Penichet, Disruption of HOX activity leads to cell death that can be enhanced by the interference of iron uptake in malignant B cells, Leukemia 24 (2010) 1555–1565.

[9] R. Morgan, P.M. Pirard, L. Shears, J. Sohal, R. Pettengell, H.S. Pandha, Antagonism of HOX/PBX dimer formation blocks the in vivo proliferation of melanoma, Cancer Res. 67 (2007) 5806–5813.
[10] L. Plowright, K.J. Harrington, H.S. Pandha, R. Morgan, HOX transcription factors are potential therapeutic targets in non-small-cell lung cancer (targeting HOX genes in lung cancer), Br. J. Cancer 100 (2009) 470–475.
[11] S.E. McGrath, A. Michael, H. Pandha, R. Morgan, Engrailed homeobox transcription factors as potential markers and targets in cancer, FEBS Lett. 587 (2013) 549–554.
[12] N.L. Martin, M.K. Saba-El-Leil, S. Sadekova, S. Meloche, G. Sauvageau, EN2 is a candidate oncogene in human breast cancer, Oncogene 24 (2005) 6890–6901.
[13] R. Morgan, A. Boxall, A. Bhatt, M. Bailey, R. Hindley, S. Langley, et al., Engrailed-2 (EN2): a tumor specific urinary biomarker for the early diagnosis of prostate cancer, Clin. Cancer Res. 17 (2011) 1090–1098.
[14] H. Pandha, K.D. Sorensen, T.F. Orntoft, S. Langley, S. Hoyer, M. Borre, R. Morgan, Urinary engrailed-2 (EN2) levels predict tumour volume in men undergoing radical prostatectomy for prostate cancer, BJU Int. 110 (2012) E287–E292.
[15] J. Hu, S. Wang, L. Wang, F. Li, B. Pingguan-Murphy, T.J. Lu, F. Xu, Advances in paper-based point-of-care diagnostics, Biosens. Bioelectron. 54 (2014) 585–597.
[16] A.D. Ellington, J.W. Szostak, In vitro selection of RNA molecules that bind specific ligands, Nature 346 (1990) 818–822.
[17] C. Tuerk, L. Gold, Systematic evolution of ligands by exponential enrichment: RNA ligands to bacteriophage T4 DNA polymerase, Science 249 (1990) 505–510.
[18] J.G. Bruno, J.L. Kiel, In vitro selection of DNA aptamers to anthrax spores with electrochemiluminescence detection, Biosens. Bioelectron. 14 (1999) 457–464.
[19] N. Hamaguchi, A. Ellington, M. Stanton, Aptamer beacons for the direct detection of proteins, Anal. Biochem. 294 (2001) 126–131.
[20] R. Joshi, H. Janagama, H.P. Dwivedi, T.M.A. Senthil Kumar, L.A. Jaykus, J. Schefers, S. Sreevatsan, Selection, characterization, and application of DNA aptamers for the capture and detection of Salmonella enterica serovars, Mol. Cell. Probes 23 (2009) 20–28.
[21] S. Tombelli, M. Minunni, E. Luzi, M. Mascini, Aptamer-based biosensors for the detection of HIV-1 Tat protein, Bioelectrochemistry 67 (2005) 135–141.
[22] W. Niu, N. Jiang, Y. Hu, Detection of proteins based on amino acid sequences by multiple aptamers against tripeptides, Anal. Biochem. 362 (2007) 126–135.
[23] N. De-los-Santos-Álvarez, M.J. Lobo-Castañón, A.J. Miranda-Ordieres, P. Tuñón-Blanco, Modified-RNA aptamer-based sensor for competitive impedimetric assay of neomycin B, J. Am. Chem. Soc. 129 (2007) 3808–3809.
[24] M. Li, X. Zhou, W. Ding, S. Guo, N. Wu, Fluorescent aptamer-functionalized graphene oxide biosensor for label-free detection of mercury(II), Biosens. Bioelectron. 41 (2013) 889–893.
[25] M. Ikanovic, W.E. Rudzinski, J.G. Bruno, A. Allman, M.P. Carrillo, S. Dwarakanath, et al., Fluorescence assay based on aptamer-quantum dot binding to bacillus thuringiensis spores, J. Fluoresc. 17 (2007) 193–199.
[26] C.C. Chang, S. Lin, C.H. Lee, T.L. Chuang, P.R. Hsueh, H.C. Lai, C.W. Lin, Amplified surface plasmon resonance immunosensor for interferon-Gamma based on a streptavidin-incorporated aptamer, Biosens. Bioelectron. 37 (2012) 68–74.
[27] S.J. Lee, B.S. Youn, J.W. Park, J.H. Niazi, Y.S. Kim, M.B. Gu, ssDNA aptamer-based surface plasmon resonance biosensor for the detection of retinol binding protein 4 for the early diagnosis of type 2 diabetes, Anal. Chem. 80 (2008) 2867–2873.
[28] L. Kashefi-Kheyrabadi, M.A. Mehrgardi, Aptamer-based electrochemical biosensor for detection of adenosine triphosphate using a nanoporous gold platform, Bioelectrochemistry 94 (2013) 47–52.
[29] A.A. Lubin, R.Y. Lai, B.R. Baker, A.J. Heeger, K.W. Plaxco, Sequence-specific, electronic detection of oligonucleotides in blood, soil, and foodstuffs with the reagentless, reusable E-DNA sensor, Anal. Chem. 78 (2006) 5671–5677.
[30] A.E. Radi, J.L.A. Sánchez, E. Baldrich, C.K. O'Sullivan, Reusable impedimetric aptasensor, Anal. Chem. 77 (2005) 6320–6323.
[31] N.J. Ronkainen, H.B. Halsall, W.R. Heineman, Electrochemical biosensors, Chem. Soc. Rev. 39 (2010) 1747–1763.
[32] C. Karuwan, A. Wisitsoraat, D. Phokharatkul, C. Sriprachuabwong, T. Lomas, D. Nacapricha, A. Tuantranont, A disposable screen printed graphene-carbon paste electrode and its application in electrochemical sensing, RSC Adv. 3 (2013) 25792–25799.
[33] S. Lee, H. Jo, J. Her, H.Y. Lee, C. Ban, Ultrasensitive electrochemical detection of engrailed-2 based on homeodomain-specific DNA probe recognition for the diagnosis of prostate cancer, Biosens. Bioelectron. 66 (2015) 32–38.
[34] H.F. Teh, H. Gong, X.-D. Dong, X. Zeng, A.L.K. Tan, X. Yang, S.N. Tan, Electrochemical biosensing of DNA with capture probe covalently immobilized onto glassy carbon surface, Anal. Chim. Acta 551 (2005) 23–29.
[35] X. Yang, S.B. Hall, S. Ngin Tan, Electrochemical reduction of a conjugated cinnamic acid diazonium salt as an immobilization matrix for glucose biosensor, Electroanal 15 (2003) 885–891.
[36] H.-E. Lee, Y.O. Kang, S.-H. Choi, Electrochemical-DNA biosensor development based on a modified carbon electrode with gold nanoparticles for influenza A (H1N1) detection: effect of spacer, Int. J. Electrochem Sci. 9 (2014) 6793–6808.
[37] H. Cai, C. Xu, P. He, Y. Fang, Colloid Au-enhanced DNA immobilization for the electrochemical detection of sequence-specific DNA, J. Electroanal. Chem. 510 (2001) 78–85.
[38] S. Tombelli, M. Minunni, E. Luzi, M. Mascini, Aptamer-based biosensors for the detection of HIV-1 Tat protein, Bioelectrochemistry 67 (2005) 135–141.
[39] G.D. McEwen, F. Chen, A. Zhou, Immobilization, hybridization, and oxidation of synthetic DNA on gold surface: electron transfer investigated by electrochemistry and scanning tunneling microscopy, Anal. Chim. Acta 643 (2009) 26–37.
[40] A. Ulianas, L.Y. Heng, S.A. Hanifah, T.L. Ling, An electrochemical DNA microbiosensor based on succinimide-modified acrylic microspheres, Sensors 12 (2012) 5445–5460.
[41] J. Pan, Voltammetric detection of DNA hybridization using a non-competitive enzyme linked assay, Biochem. Eng. J. 35 (2007) 183–190.
[42] L. Dykman, N. Khlebtsov, Gold nanoparticles in biomedical applications: recent advances and perspectives, Chem. Soc. Rev. 41 (2012) 2256–2282.